High-Performance Programmable Memory Devices Based on Co-Doped $BaTiO_3$

*Zhibo Yan, Yanyan Guo, Guoquan Zhang, and J.-M. Liu**

Recently, resistive random access memory (RRAM) devices have attracted great attentions for a variety of advantages such as high-density, high-speed, low-power, and thus promising applications in next-generation nonvolatile memory technology.[1–4] The memory effect is realized through switching between high resistance state (HRS) and low resistance state (LRS), controlled by electric field with either opposite polarity (bipolar) or different magnitude (unipolar). In understanding this resistive switching (RS) effect, quite a number of microscopic mechanisms have been proposed, while the formation/rupture of conductive filaments in insulating matrix as one of the major switching mechanisms has been intensively studied.[3–5] It is demonstrated that the composition of the conductive filaments and their formation/rupture are remarkably materials-dependent, thus the RRAM device performance is materials dependent too. For the favored device performance, complex transition metal oxides may be the most promising candidates.[3] The strong correlation of electrons in these oxides brings out rich competing phenomena between various electronic phases in a delicate balance, allowing a phase change and thus dramatic change of the electrical property, e.g. resistance, in response to a minute external perturbation, e.g., an applied electric field.[6] Furthermore, the atomic and/or electronic reconstruction at grain boundaries or doping centers in these oxides enriches the electronic phases, providing an opportunity for advanced electronics.[7,8]

By an extensive testing of various oxide materials in terms of the RRAM performance, we eventually choose ferroelectric $BaTiO_3$ for the present study. A low-doping at the Ti-site can introduce itinerant electrons, leading to the presence of inhomogeneous state, i.e., the coexistence of metallic and ferroelectric phases.[9] As an electric field is applied on this inhomogeneous state, the local Joule heating induced by inhomogeneous current distribution may lead to the reconstruction of local atomic and/or electronic phases, causing the large change in conductance.[8,10] Besides, earlier works suggested that the ferroelectric displacements will also change the electronic structure.[11] Hence, $BaTiO_3$-based materials offer a good opportunity to develop the RRAM devices with more promising functionalities. In this work, we fabricate 5at% Co-doped $BaTiO_3$ (BTCO) films. The unipolar RS characteristics with the endurance of more than 10^5 and switching time of less than 10 ns in addition to other preferred properties are demonstrated.

We fabricated the BTCO-based memory cell, with the entire materials stack (thicknesses) of Au(400 nm)/BTCO(400 nm)/Pt(300 nm)/Ti(50 nm)/SiO_2(500 nm)/Si. The X-ray diffraction (XRD) data indicate that the BTCO films are polycrystalline, as shown in **Figure 1**a. Figure 1b and c depict a schematic drawing of the measurement configuration and the scanning electron

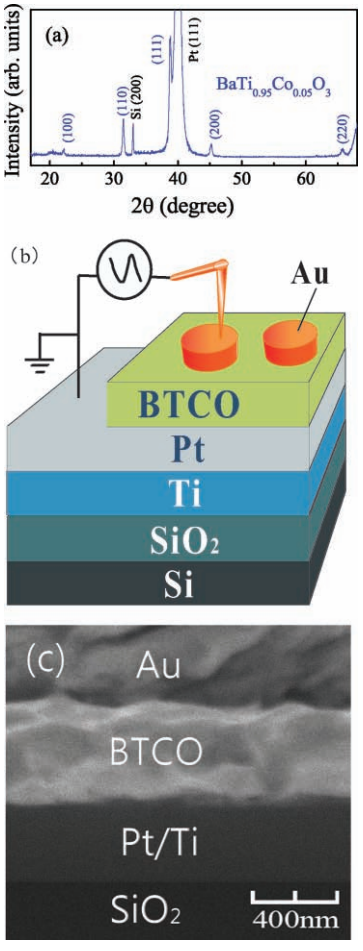

Figure 1. (a) XRD data of the as-prepared $BaTi_{0.95}Co_{0.05}O_3$ film. (b) A schematic drawing of the measurement configuration. (c) Cross-section SEM image of a memory cell.

Z. B. Yan, Y. Y. Guo, G. Q. Zhang, Prof. J.-M. Liu
Laboratory of Solid State Microstructures
Nanjing University
Nanjing 210093, P. R. China
E-mail: liujm@nju.edu.cn
Prof. J.-M. Liu
School of Physics
South China Normal University
Guangzhou 510631, P. R. China
Z. B. Yan, Y. Y. Guo, G. Zhang, Prof. J.-M. Liu
International Center for Materials physics
Chinese Academy of Sciences
Shenyang 110016, P. R. China

DOI: 10.1002/adma.201004306

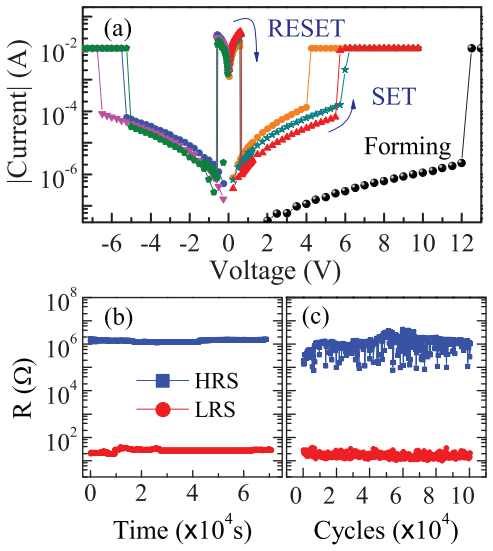

Figure 2. (a) Typical current-voltage (*I*–*V*) characteristics. After the forming sweep (0 → 15 V), six consecutive RESET-SET cycles are displayed, with the sweep (0→±1.5 V) for RESET and the sweep (0→±10 V) for SET. (b) Retention data of HRS and LRS after the RESET and SET, respectively, readout at 0.1 V. (c) Endurance data for 10^5 consecutive RESET-SET cycles, readout at 0.1 V.

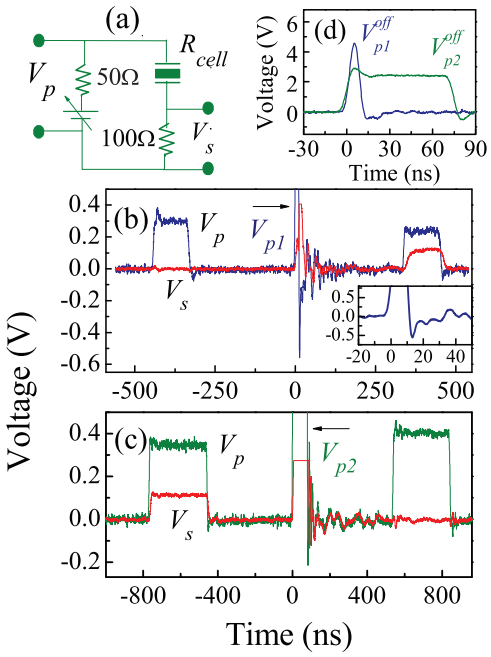

Figure 3. Programming speed test of the memory cell. (a) Wiring diagram, (b) Waveforms of V_s and V_p with V_{p1} at time t~0. Inset: the magnified curve of V_p. (c) Waveforms of V_s and V_p with V_{p2} at time t ~ 0. (d) V_{p1}^{off} and V_{p2}^{off} pulses: the off-load outputs of the switching pulse V_{p1} and V_{p2}, respectively.

microscopy (SEM) image of the cross-sectional profile of the as-prepared thin film, respectively.

In our experiment, the fresh memory cells are always at the HRS, with a resistance of ~10 MΩ. In order to obtain a steady reversible resistive switching, a forming process is needed in prior to the testing. **Figure 2**a shows the typical current-voltage (*I*–*V*) characteristics of the memory cell. The voltage sweeping from 0 → ±10 V, with steps of 0.25 V and current compliance of 10 mA, was used to SET the cell from the HRS to the LRS, while the other sweep of 0 → ±1.2 V, with steps of 0.02 V and without current compliance, was used to RESET the cell back to the HRS. Our experiments indicate that the critical voltages, V_{SET} and V_{RESET}, at which the resistance is abruptly switched from the HRS to the LRS and then back to the HRS, respectively, do not depend on the polarity, showing the unipolar RS characteristics. The SET and RESET transitions typically occur at V_{set} ~ 3–7.5 V and V_{reset} ~ 0.5–0.65 V, respectively, and the typical resistance ratio, R_{HRS}/R_{LRS}, readout at 0.1 V, is higher than 10^4. The retentions of HRS and LRS are maintained over 7×10^4 s without any decaying, and the endurance remains non-degradable even after the 10^5 consecutive SET-RESET cycles, as shown in Figure 2b and c respectively.

The high programming speed is the attractive merit of BTCO-based memory cells. To test the switching speed, the memory cell in series with a resistance R_s = 100 Ω was connected to a programming pulse generator, and then the output of pulse generator (V_p) and the voltage drop across the series resistance (V_s) were measured by oscilloscope, as shown in **Figure 3**a. In order to switch the memory cell and probe the variation of resistance state, the pulse train was generated, in which a high switching pulse (used for SET or RESET) was imposed in-between the two small probing pulses (used for reading resistance state). Figure 3b and c indicate the entire waveforms of V_p and V_s. The <0.4 V pulses of ~120 ns in Figure 3b and the <0.5 V pulses of ~300 ns in Figure 3c served as probing pulses to measure the resistance state. To capture the whole waveforms of switching pulses V_{p1} and V_{p2}, we also measured the off-load outputs of V_{p1} and V_{p2}, i.e., V_{p1}^{off} and V_{p2}^{off} respectively. Although the variation of load resistance will change the amplitude of V_p due to the impedance mismatching between the pulse generator and the measuring circuit, the waveform shape remains unchanged and its amplitude can be calculated (see the supplementary material for the detail discussion). Hence, the pulse widths (FWHM) of V_{p1}^{off} and V_{p2}^{off}, i.e., those of V_{p1} and V_{p2}, are ~8 ns and ~69 ns respectively, as shown in Figure 3d.

According to the relationship of $R_{cell} = R_s(V_p - V_s)/V_s$ (see Figure 3a), a small V_p but V_s ~0 suggest the large R_{cell}, i.e., the HRS, while both small but finite V_s and V_p suggest the LRS on the contrary. Hence, Figure 3b and c clearly indicate that the resistance state is switched from the HRS to the LRS under the pulse of V_{p1}, and switched from the LRS to the HRS under the pulse of V_{p2} respectively. It is calculated that $V_{p1} \sim V_{p1}^{off}$, i.e.,~4.6 V, is dropped across the memory cell for HRS→LRS switching, and $V_{p2} \sim 0.71 V_{p2}^{off}$, i.e., ~1.7 V, is dropped across the memory cell for LRS→HRS switching. Although there is oscillating effect after imposing the pulse of V_{p1}, the first and highest oscillating peak (~ −0.56V), magnified in the inset of Figure 3b, is sufficiently small so that the resistance state remains unaffected. After imposing the pulse of V_{p2}, the first and highest oscillating peak (~ −0.21V) is also sufficiently small so that the resistance state remains unaffected. That implies that the switching is only operated by V_{p1} or V_{p2}. Hence, it is safe to argue that the switching speed is less than 10 ns for SET and

less than 70 ns for RESET. These data demonstrate that BTCO is indeed a promising candidate for resistive memory applications.

Similar to earlier reports, the unipolar resistive switching is argued to achieve mainly by the formation and rupture of conductive filament, while other mechanisms may also be involved. To verify the inhomogeneous conduction of memory cell and therein the filament model, we prepared an Au top electrode to SET the memory cell into the LRS, then cut the electrode into two parts (*TE-I* and *TE-II*) using the probe tip, and measured the resistance between the bottom electrode and *TE-I* or *TE-II*, as shown in **Figure 4**a. The dramatically different resistances measured with the *TE-I* and *TE-II* indicates the inhomogeneous conductivity. The resistance measured with the *TE-I* is as small as that at the LRS, suggesting the presence of conductive filaments inside the region between *TE-I* and the bottom electrode. The resistance measured with the *TE-II* is even higher than that before the SET process, because no filament is available below the *TE-II* and the electrode area is reduced in this part. This experiment seems to confirm the filament model. Besides, the metallic behavior of the filament and the insulating behavior of matrix are also demonstrated by the monotonous increasing and decreasing tendencies in the temperature-resistance curves for the LRS and HRS, respectively, as shown in Figure 4(b).

To further understand the conduction mechanisms, the *I–V* relationships in several models,[12–15] including $I \propto V$ for the Ohmic law, $I \propto V^2$ for the space charge limited current (SCLC), $\ln(I) \propto \mathrm{Sqrt}(V)$ for the Schottky emission, $\ln(I/V) \propto \mathrm{Sqrt}(V)$ for the Poole–Frenkel (PF) emission, and $\ln(I/V^2) \propto 1/V$ for the Fowler-Nordeim tunneling, are used to fit the typical *I–V* data. Figure 4c and its inset show the best fittings for the HRS. The low voltage region is dominated by the Schottky emission at the interface between the electrodes and BTCO film, while the high voltage region is controlled by the bulk-limited PF emission.

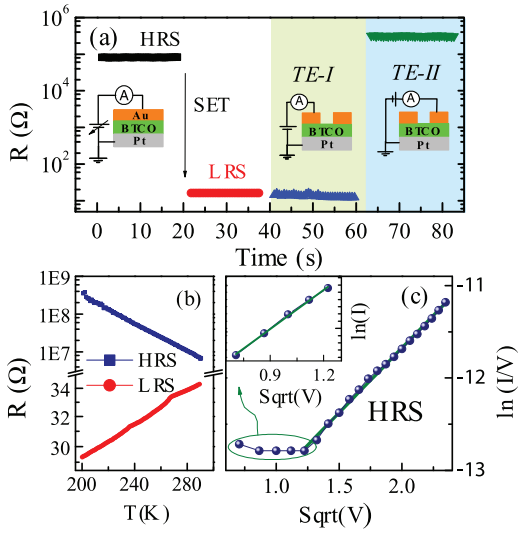

Figure 4. (a) Resistances measured upon various configurations. The top electrode (*TE*) was cut into *TE-I* and *TE-II* by the probe tip after the cell was switched from HRS to LRS by the SET process. (b) Temperature dependent resistance for HRS and LRS. (c) Typical $\mathrm{Sqrt}(V)$-$\ln(I/V)$ plot for HRS. Inset: $\mathrm{Sqrt}(V)$-$\ln(I)$ plot for HRS at low field region. Green lines: the linear fitting curves.

The PF emission comes from the electric field induced suppression of the Coulomb potential barrier for trapped sites.[12,13] The fitting results suggest that as the memory cell is switched from the HRS to the LRS under high electric field, the Coulomb potential barrier suppression should be replaced by phase transition that favor the electronic conduction, because the metallic state appears in the local region.[6,8] While for the LRS, the local Joule heating plays a dominate role at high voltage region, verified by $V/I \propto I^2$, similar to earlier investigations.[13] The local large thermal excitation induced by the Joule heating melts those earlier formed conductive filaments, leading to the RS from the LRS back to the HRS.[16] Under such two different mechanisms, the difference in pulse width for SET and RESET can be understood (see supplementary material for the details).

For the phase change mentioned above, the atomic dislocations and/or the electronic reconstruction at local regions are important ways.[5,6,8] Under an electric field, the migration of oxygen vacancies/ions favors the formation of metallic suboxides in the local regions, leading to the insulator-to-metal transition.[3,4,8] Besides, the remarkable Joule heating in some of those metallic regions may provide thermal excitation for the thermally activated diffusion of electrically migrated oxygen vacancies, which in turn destroys the metallic nature of those regions and causes the recovery of the HRS. In the BTCO films, the easily varied valence of Co ions,[17] oxygen vacancies,[18,19] and local itinerant electrons induced by the Co-doping, all favor the electrical migration or the thermal diffusion of oxygen vacancies/ions in local region under high electric field or large Joule heating respectively.[9]

The conductivity in $BaTiO_3$ may rely also on the small-polaron hopping.[20] The reduction of the concentration of oxygen vacancies raises the activation energies for hopping and as a result reduces the conductivity, and vice visa.[21] To vary the oxygen vacancies concentration, we annealed the BTCO film at 300, 450, 600, or 800 (°C) for 5 minute in oxygen atmosphere, and then measured the resistances with 0.1 V after the deposition of Au top electrode at room temperature. The data (shown in the Supplementary materials) indicates that the initial resistance of BTCO decreased after annealing at 300 °C or at 450 °C. This may be the indication that the Ti migrates through the Pt bottom electrode and can therefore serve to chemically reduce the BTCO and actually create vacancies.[22] Upon increasing the annealing temperature to 600 °C and then 800 °C, the initial resistance of BTCO film increases dramatically and eventual becomes much higher than that before the annealing experiment. This suggests that the oxygen annealing away vacancies is dominant and the oxygen vacancies are reduced after the annealing at 800 °C.

To study how the reduction of pre-existing oxygen vacancies in BTCO film influences the RS characteristics,[23] we performed the forming procedure and the SET-RESET cycling test after the oxygen annealing at 800 °C. The data indicate that the endurance becomes worse (<10^3 cycles), and the fluctuations of V_{SET}, V_{RESET}, R_{HRS}, and R_{LRS}, become more serious. It is noted that the large fluctuations of V_{SET} and V_{RESET} may cause the failure of reversible RS and as a result reduce the endurance performance. In this case, we re-test the SET-RESET cycles with broader voltage sweeping ranges: 0 → 1.5 V for RESET and 0 → 20 V for SET. As a consequence, the endurance can be enhanced up to ~10^4 cycles.

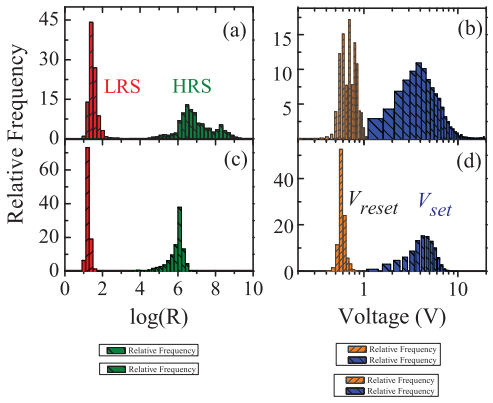

Figure 5. (a,b) Distributions of $log(R_{LRS})$, $log(R_{HRS})$, V_{SET}, and V_{RESET} after the oxygen annealing at 800 °C, evaluated from the statistics on 10^4 consecutive RESET-SET cycles. (c,d) Distributions of $log(R_{LRS})$, $log(R_{HRS})$, V_{SET}, and V_{RESET} without the annealing, evaluated from the statistics on 10^5 consecutive RESET-SET cycles. The binning sizes of both $log(R_{LRS})$ and $log(R_{HRS})$ are 0.2, while those of V_{RESET} and V_{SET} are 0.05 V and 0.5 V, respectively.

Based on the cycling data, the relative distributions of $log(R_{LRS})$ and $log(R_{HRS})$ plus V_{SET} and V_{RESET}, are shown in **Figure 5**(a) and (b) respectively. For the comparison, these distributions in prior to the oxygen annealing are also shown in Figure 5(c) and (d), in which the statistics was done on the data of 10^5 SET-RESET cycles. It is seen that after the annealing processing, the reduction of pre-existing oxygen vacancies in BTCO leads to the up-shift of the most probably $log(R_{HRS})$ and $log(R_{LRS})$ from 6.1 to 6.5 and 1.15 to 1.45, respectively. Due to the less pre-existing vacancies that can participate in the resistance change, additional atomic dislocations should be produced by electric field to form the filaments,[19] which may be the reason for the slight increase of the most probably V_{set}. Similarly, the higher most probably V_{reset} should be needed to diffuse such additionally generated dislocations for disconnecting the filament. Furthermore, besides the electrical migration and thermal diffusion of pre-existing oxygen vacancies/ions, the generation and annihilation of these electric field induced dislocations in a random way should complicate the occurrence of RS and introduce additional disturbance, which will broaden the distributions of $log(R_{LRS})$, $log(R_{HRS})$, V_{SET}, and V_{RESET} etc. These variations clearly indicate that the pre-existing oxygen vacancies with sufficiently high density seem necessary for the stable RS characteristics.

In summary, we have fabricated non-volatile memory cells using the Co-doped $BaTiO_3$ thin films as active layers. The stable unipolar resistive switching characteristics, with a resistance ratio over 10^4, retention time longer than 7×10^4 s, endurance over 10^5 cycles, and switching speed less than 10 ns/70 ns for the SET/RESET, have been demonstrated. The resistive switching memory effect originates from the formation and the rupture of conductive filaments, which may be realized by the electrical migration and thermal diffusion of oxygen vacancies respectively. The concentration of oxygen vacancies influences the RS characteristics dramatically.

Experimental Section

Synthesis: The polycrystalline $BaTi_{0.95}Co_{0.05}O_3$ (BTCO) ceramic target with 2 cm in diameter was synthesized by the solid-state reaction method from $BaCO_3$, TiO_2, and Co_2O_3 with 99.99% purity. Then this target was used to deposit BTCO films on $Pt/Ti/SiO_2/Si$ substrates by pulsed laser deposition using a KrF excimer laser with wavelength of 248 nm. The laser energy density, laser repetition rate, oxygen ambient pressure, and growth temperature are 2 J cm^{-2}, 2 Hz, 15 Pa, and 800 °C, respectively. The Au top electrodes with 100 μm in diameter were deposited by rf magnetron sputtering with a shadow mask.

Characterization: The crystallization of BTCO films is confirmed by X-ray diffraction (XRD) technologies, and the morphology and thickness of the films were investigated by scanning electron microscopy (SEM). The current-voltage (*I–V*) characteristics and the retention and endurance performances were measured by the two-probe method using a Keithley 236 source meter at room temperature. For obtaining more accurate quasi-static *I–V* characteristic, the voltage sweeps were applied in the pulse stair mode with a pulse width of 1ms and a pulse separation of 100 ms, which was used to have enough time to dissipate the historical accumulation of Joule heat during the voltage sweeps. For testing the switching speed, Agilent 33250B signal generator was used to produce the pulse trains, and LeCroy WR62Xi oscilloscope was used to measure the waveforms of V_p and V_s simultaneously. In order to program the proper pulse train, proper voltage drops across the memory cell were firstly chosen according to the switching characteristics, and then the amplitudes that would be programmed in Agilent 33250B were calculated (detaily described in the supplementary material). The temperature dependent resistance was measured in the cryogenic equipment, with 0.1 V and a temperature ramping rate of 2 K min^{-1}.

Acknowledgements

This work was supported by the National Key Projects for Basic Research of China (2011CB922101 and 2009CB623303) and the National Natural Science Foundation of China (50832002, 51031004, 11074113).

Received: November 22, 2010
Published online: February 15, 2011

[1] K. Shibuya, R. Dittmann, S. Mi, R. Waser, *Adv. Mater.* **2010**, *22*, 411.
[2] M. Janousch, G. I. Meijer, U. Staub, B. Delley, S. F. Karg, B. P. Andreasson, *Adv. Mater.* **2007**, *19*, 2232.
[3] A. Sawa, *Mater. Today* **2008**, *11*, 28.
[4] R. Waser, M. Aono, *Nature Mater.* **2007**, *6*, 833.
[5] J. P. Strachan, M. D. Pickett, J. J. Yang, S. Aloni, A. L. David Kilcoyne, G. Medeiros-Ribeiro, R. Stanley Williams, *Adv. Mater.* **2010**, *22*, 3573.
[6] H. Takagi, H. Y. Hwang, *Science* **2010**, *327*, 1601.
[7] J. Mannhart, D. G. Schlom, *Science* **2010**, *327*, 1607.
[8] D.-H. Kwon, K. M. Kim, J. H. Jang, J. M. Jeon, M. H. Lee, G. H. Kim, X.-S. Li, G.-S. Park, B. Lee, S. Han, M. Kim, C. S. Hwang, *Nature Nanotech.* **2010**, *5*, 148.
[9] T. Kolodiazhnyi, M. Tachibana, H. Kawaji, J. Hwang, E. Takayama-Muromachi, *Phys. Rev. Lett.* **2010**, *104*, 147602.
[10] U. Russo, D. Ielmini, C. Cagli, A. L. Lacaita, *IEEE Trans. Electr. Dev.* **2009**, *56*, 193.
[11] J. Velev, C.-G. Duan, K. Belashchenko, S. Jaswal, E. Tsymbal, *Phys. Rev. Lett.* **2007**, *98*, 137201.
[12] S. J. Wang, M. O. Lai, L. Lu, *J. Phys. D: Appl. Phys.* **2010**, *43*, 305401.
[13] Z. B. Yan, S. Z. Li, K. F. Wang, J.-M. Liu, *Appl. Phys. Lett.* **2010**, *96*, 012103.

[14] J.-G. Park, W.-S. Nam, S.-H. Seo, Y.-G. Kim, Y.-H. Oh, G.-S. Lee, U.-G. Paik, *Nano Lett.* **2009**, *9*, 1713.
[15] J. S. Choi, J. S. Kim, I. R. Hwang, S. H. Hong, S. H. Jeon, S. O. Kang, B. H. Park, D. C. Kim, M. J. Lee, S. Seo, *Appl. Phys. Lett.* **2009**, *95*, 022109.
[16] S. Chang, J. Lee, S. Chae, S. Lee, C. Liu, B. Kahng, D. W. Kim, T. Noh, *Phys. Rev. Lett.* **2009**, *102*, 026801.
[17] H. Shima, F. Takano, H. Akinaga, Y. Tamai, I. H. Inoue, H. Takagi, *Appl. Phys. Lett.* **2007**, *91*, 012901.
[18] Q. Liu, S. Long, W. Wang, Q. Zuo, S. Zhang, J. Chen, M. Liu, *IEEE Electron Dev. Lett.* **2009**, *30*, 1335.
[19] H. Zhang, B. Gao, B. Sun, G. Chen, L. Zeng, L. Liu, X. Liu, J. Lu, R. Han, J. Kang, B. Yu, *Appl. Phys. Lett.* **2010**, *96*, 123502.
[20] R. Scharfschwerdt, A. Mazur, O. F. Schirmer, H. Hesse, S. Mendricks, *Phys. Rev. B* **1996**, *54*, 15284.
[21] J. P. Boyeaux, F. M. Michel-Calendini, *J. Phys. C: Solid State Phys.* **1979**, *12*, 545.
[22] J. J. Yang, J. P. Strachan, Q. Xia, D. A. A. Ohlberg, P. J. Kuekes, R. D. Kelley, W. F. Stickle, D. R. Stewart, G. Medeiros-Ribeiro, R. S. Williams, *Adv. Mater.* **2010**, *22*, 4034.
[23] Y. Nian, J. Strozier, N. Wu, X. Chen, A. Ignatiev, *Phys. Rev. Lett.* **2007**, *98*, 146403.